Local Convective Boiling Heat Transfer And Pressure Drop Of Nanofluid In Narrow Rectangular Channels

Mounir Boudouh, Hasna Louahlia Gualous, Michel de Labachelerie

Accepted Manuscript

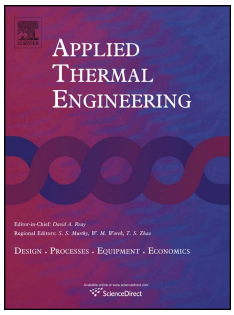

Title: Local Convective Boiling Heat Transfer And Pressure Drop Of Nanofluid In Narrow Rectangular Channels

Authors: Mounir Boudouh, Hasna Louahlia Gualous, Michel De Labachelerie

PII: S1359-4311(10)00274-7

DOI: 10.1016/j.applthermaleng.2010.06.027

Reference: ATE 3158

To appear in: *Applied Thermal Engineering*

Received Date: 7 November 2009

Revised Date: 17 March 2010

Accepted Date: 29 June 2010

Please cite this article as: M. Boudouh, H.L. Gualous, M. De Labachelerie. Local Convective Boiling Heat Transfer And Pressure Drop Of Nanofluid In Narrow Rectangular Channels, Applied Thermal Engineering (2010), doi: 10.1016/j.applthermaleng.2010.06.027

LOCAL CONVECTIVE BOILING HEAT TRANSFER AND PRESSURE DROP OF NANOFLUID IN NARROW RECTANGULAR CHANNELS

Mounir Boudouh, Hasna Louahlia Gualous, Michel De Labachelerie

FEMTO ST Institute, Micro Nano Systems & Science department, CNRS-UMR 6174

UTBM, rue Thierry Mieg, 90010 Belfort, France.

Abstract

This paper reports an experimental study on convective boiling heat transfer of nanofluids and de-ionized water flowing in a multichannels. The test copper plate contains 50 parallel rectangular minichannels of hydraulic diameter 800 µm. Experiments were performed to characterize the local heat transfer coefficients and surface temperature using copper-water nanofluids with very small nanoparticles concentration. Axial distribution of local heat transfer is estimated using a non-intrusive method. Only responses of thermocouples located inside the wall are used to solve inverse heat conduction problem. It is shown that the distribution of the local heat flux, surface temperature, and local heat transfer coefficient are dependent on the axial location and nanoparticles concentration. The local heat transfer coefficients estimated inversely are close to those determined from the correlation of Kandlikar and Balasubramanian [32] for boiling water. It is shown that the local heat flux, local vapor quality, and local heat transfer coefficient increase with copper nanoparticles concentration. The surface temperature is high for de-ionized water and it decreases with copper nanoparticles concentration.

Keywords : Nanofluid, minichannel, flow boiling, local heat transfer, nanoparticles.

Corresponding author. hasna.gualous@femto-st.fr, Tel.: +33-3-8458-3645, fax: +33-3-8458-3636

1. INTRODUCTION

A significant improvement in the performance of microelectronic devices was accompagned by the increase in heat generation. For this reason, various new boiling cooling systems have been developped and required the extensive investigations for convective flow boiling in microchannels and minichannels. Flow boiling at low Reynolds number has been used extensively in many practical applications where micro and minichannels were employed, such as compact cooling systems for electronic chips and compact heat exchangers. Boiling contributes greatly to enhance the thermal performance of each microchannel heat sink by providing high heat transfer at very low flow rates, and minimizing the temperature gradients. Heat transfer and pressure drop of convective flow boiling inside microchannels and minichannels are influenced by several physical parameters such as : flow patterns [1], hydrodynamic instabilities [2], concentration of mixing solid nanoparticles in the base working fluid [3], convective effect due to the Reynolds number [4], two-phase flow structure [5], working fluid properties [6], forces acting the liquid-vapor interface [7].

The physical properties of working fluids in cooling systems play an important role to achieve better cooling performance. The thermal conductivity is the first limitation for enhancing heat transfer. It is known that thermal conductivity for conventional fluids is very low compared to solids. It was confirmed by the numerous experimental and theoretical studies [8-11], that uniform suspension of solid nanoparticles into base fluids (i.e. nanofluids) enhanced fluid thermal conductivities and improved fluid heat transfer performance. Thermal properties of nanofluids depend on the nanoparticles volume fraction, size and shape, type of base fluid, and nanoparticles material. According to the previous studies [12-14], the thermal conductivity of nanofluid could be hundreds of times greater than those of base fluids. Extensive research has been conducted to understand the heat transfer coefficient and nanofluids properties for single and boiling flow. Convection heat transfer was studied for various nanofluids with various suspended nanoparticles: Al2O3-water [15-17], CuO-water [18], SiO2-water [19], TiO2-water [20], Ag-water [21], etc. Research has shown that degradation of pool boiling heat transfer was obtained with nanofluids compared to base fluids. Nanofluids show a great enhancement in critical heat flux particularly at very low nanoparticles volume fraction [22]. You et al. [23] have reported that pool boiling critical heat flux was enhanced to 200% using Al_2O_3-water nanofluids at 0.0007% volume fraction. The degradation of heat transfer coefficient and enhancement of critical heat flux with nanofluids are probably due to the sedimentation of nanoparticles which change surface rugosity.

Nanofluids are the innovative idea for thermal engineering. Although, many questions remain unanswered and need researching. Until now major researches on boiling heat transfer characteristics of nanofluid are

conducted on pool boiling heat transfer [24-27]. From review of the open literature, it is clear that there is no published study on local heat transfer for convective boiling nanofluid in micro or minichannel. It is clear that reducing hydraulic diameter of channels in cooling systems offer appreciable advantages such as high heat transfer coefficient, high compactness, and small working fluid quantity. Additionally, using nanofluids as a working fluid contributes also to enhance heat transfer obtained by reducing hydraulic diameter. Thus, several classifications for transition from microscale to macroscale heat transfer have been proposed. For phase change heat transfer, Cheng et al. [28] have proposed a classification of microchannels based on Bond number: (i) microchannel ($Bo < 0.05$), (ii) minichannel ($0.05 < Bo < 3$), and (iii) macrochannel ($Bo > 3$). Bond number takes into account the effects of temperature, pressure, and physical properties of working fluid. It is given by:

$$Bo = \left(\frac{D_h}{l_c} \right)^2 \quad (1)$$

where D_h is the hydraulic diameter, l_c is the capillary length defined as :

$$l_c = \sqrt{\frac{\sigma}{g(\rho_l - \rho_v)}} \quad (2)$$

Using water as the working fluid, the capillary length is about 2.72 mm (at 373K). According to the classification of Cheng et al. [1], channels with hydraulic diameter between 600µm-4720 µm are considered minichannels.

The present study investigates the local pressure drop and local heat transfer coefficient for convective boiling by combining two advantages: (i) the reduction of channel diameter, and (ii) the use of nanofluids with the low nanoparticles volume fraction because it involves probably no sedimentation and no penalty of nanoparticles deposition on heat exchange surface. The main objective of this study is to determine nanofluids local performance for convective boiling in minichannels with a hydraulic diameter of 800µm ($Bo = 0.086$). The local heat transfer coefficient, local surface temperature, and local heat flux are investigated for different nanoparticles volume fractions. The effect of copper nanoparticles concentrations on local pressure drop is studied.

2. EXPERIMENTAL APPARATUS

As shown in Figure 1, the experimental device has been designed to measure local heat transfer coefficients and to visualize flow patterns for convective boiling inside parallel microchannels. For this investigation, the

experimental set up consists of the microchannels test section (evaporator) and working fluid loop. The liquid in the tank (1) is pumped by the magnetic gear pump (3) with microprocessor control type MCP-Z standard, which is also used as a flow meter. A 2µm filter (2) is used to eliminate any dust or microparticles in the working fluid. The gear pump (3) drives the fluid from the tank entrance to the test section (5). The mass flux is adjusted through the regulating valves. The flow meter is calibrated for different liquid flow rates by weighing the collected liquid during a known period of time. The uncertainty in the mass flow is about 1.3%. After passing the microchannels test section, the working fluid becomes in two-phase flow and it is led into the heat exchanger (7) in which it is cooled before returning in the liquid tank (1). The temperature of the working fluid in the tank (1) is controlled using an electrical heater associated with a temperature controller. The bulk temperatures of the test section entrance and exit are measured using chromel-alumel microthermocouples (K-type, 75µm). Pressures are measured at parallel minichannels entrance and exit by strain gage type pressure transducers (4) and (6) with response time of 2 ms and accuracy of 0.25%. Measured data including mass flux, pressure and temperatures are acquired by Labview data acquisition system and a computer (8).

2.1. Test section and instrumentation

As shown in figure 2a, the test module is made from a square copper block 220x220x10 mm^3 into which a series of 50 parallel minichannels are machined on its top side. Each channel has a rectangular cross section (2000µm of width and 500µm of height) and a length of 160 mm. The distance between the center lines of any two adjacent channels is of 4 mm (figure 2b). The flow channels are formed by covering the copper plate top side with a polycarbonate plate of 220x220x4 mm^3 which is also used as an insulator and a transparent cover in order to visualize the boiling flow patterns. The parallel minichannels are heated by a rectangular silicone heating panels of 200x200x4 mm^3 which used to simulate the heat source (figure 3a). The heating system is placed at the copper plate bottom side. The heater system is coated with a second copper plate 200x200x4mm^3. These two copper blocks are screwed into place such they made good contact with the heater source. Precautions were taken to achieve uniform distribution of heat flux at the upper surface of the heat source. The heating panel was energized with a direct current power supply and it has 400 W of total power. The input voltage and current are controlled by a power supply and measured with an accuracy of 1%. As shown in figure 3a, thermal insulating layers (30mm thick) of PTFE with thermal conductivity 0.3 W/mK are put on all faces of the test section except the top side in order to minimize the heat losses which estimated to be lower than 7%.

The inner wall temperatures of the first channel (figure 3b) are measured by microthermocouples (K-type, 75µm) located along the channels wall. A total of 14 microthermocouples are located on the bottom side of the first channel as shown in figure 3c. Thermocouples are placed into holes drilled into the first channel of the test section. They were soldered in place by a high conductivity material between the wall and microthermocouples. As shown in figure 4, microthermocouples were placed in axial direction and in two normal locations of the first channel. Seven microthermocouples were placed at 0.5 mm below the wetted surface and at axial distances 8, 26, 44, 62, 99, 117, 135 mm from the channel inlet. Seven microthermocouples were placed at 8.5 mm below the heat exchange surface and at axial distances 11, 30, 48, 66, 103, 121, 139 mm from the channel inlet.

In this work, microthermocouples calibration is conducted by comparing the temperatures measured by microthermocouples and a precision sensor probes (±0.03°C). The calibration procedure consists to maintain the microthermocouples at a known temperature through a precision sensor probe and to record the microthermocouples responses using a labview data acquisition system. The procedure is repeated for different known temperatures. Figure 5 shows a comparison of temperatures measured by a microthermocouple and precision sensor probe. All the measured temperatures were corrected using the precision sensor probe responses as reference.

3. EXPERIMENTAL PROCEDURE AND DATA REDUCTION

To understand the physical phenomena, experimental installation and local instrumentation have been developed and some experiments were conducted. For all tests, the heat exchange surface is oriented vertically. The liquid in the tank is first preheated to the required temperature. The liquid flow rate is adjusted with the regulating valve at the desired value. The total power supplied to the heater source is set at a maximum value. When the boiling phenomenon appears and the wall temperatures become steady, the liquid flow rate or heat flux of the power source is varied and the same procedure is repeated. For each fixed operating conditions, the test section is heated and the temperatures are monitored continually. The local surface temperature and heat flux are determined by solving inverse heat conduction problem (IHCP) using only wall temperature measurements. Experiments are performed with deionized water and nanofluids.

Experimental results presented in this paper are treated only in steady state. The local heat transfer coefficient of each axial location along the channel length is determined from the local heat flux ($q_{channel,z}$) and local surface temperature ($T_{s,z}$) as follows :

$$h_z = \frac{q_{channel,z}}{T_{s,z} - T_f} \quad (3)$$

where T_f is the bulk mean temperature; it is equal to T_{sat} when boiling fluid is in the saturated state. $q_{channel,z}$ and $T_{s,z}$ are obtained by solving IHCP. This procedure offers the appreciable advantages : (i) $q_{channel,z}$ is estimated by taking into account the local heat loss, (ii) axial surface temperature is determined using non-intrusive method, (iii) $q_{channel,z}$ and $T_{s,z}$ are assumed to be variable along the flow direction due to the boiling flow patterns.

3.1 Determination of the local heat transfer coefficient

The inverse analysis has been applied to obtain the unknown thermal boundary conditions at the heat transfer surface of the minichannel. The numerical computations and a simple instrumentation using microthermocouples inside the channel wall are used to estimate the local surface temperature and local heat flux. Physical model assumes that two phase flow is two-dimensional and treats only the steady heat transfer for boiling flow in the minichannel. The mathematical model of a heat conduction process in a hollow minichannel considers a copper plate of length L and thickness E. On the bottom surface of the plate, the heat flux is assumed to be uniform and equal to the power supply. On the heat exchange surface, the local heat flux and surface temperature were unknown. All the other surfaces are assumed to be insullated and no heat flux is dissipated.

The physical model is defined by:

$$\frac{\partial^2 T}{\partial z^2} + \frac{\partial^2 T}{\partial y^2} = 0 , \quad (4)$$

where $0 \le z \le L$, $0 \le y \le E$

$$\frac{\partial T}{\partial z}(0, y) = 0 \quad (5)$$

$$\frac{\partial T}{\partial z}(L, y) = 0 \quad (6)$$

$$\lambda_w \frac{\partial T}{\partial y}(z, 0) = q_w \quad (7)$$

$$\lambda_w \frac{\partial T}{\partial y}(z, E) = q_{channel,z} \quad (8)$$

where y is the normal vector of the heat exchange surface, λ_w is the thermal conductivity of the copper wall ($\lambda_w = 389\,W/m^2K$). $q_{channel,z}$ is the unknown surface heat flux.

The finite difference method is employed in the numerical analysis process. The conjugate gradient algorithm

for estimating simultaneously the unknown surface heat flux and temperature is developped [29]. The IHCP is transformed into the solution of three problems, namely, direct, sensitivity, and adjoint problems. These problems are solved numerically and the results are used in the conjugate gradient method for inverse calculations. The numerical algorithm used for solving IHCP was detailled for cylindrical geometry in references [30-31] and will not be repeated her.

The numerical procedure is verified by using a known heat flux (also called exact heat flux) which is assumed variable along the minichannel axial direction. The bottom surface is assumed to be at the uniform heat flux. The wall temperatures are computed at the measured locations from the direct problem. These temperatures are used in the inverse procedure to minimize the residual functional and to estimate the local heat flux. The estimated values are closed to the exact heat flux as shown in references [30] and [31].

3.2 Determination of the local vapor quality

In order to quantify the local vapor mass qualities along the channel length, the energy balance equation between the inlet and outlet of each subsection is used. The local fluid temperature is assumed to be equal to the surface temperature that estimated by inverse heat conduction problem.

$$x_{v,z} = x_{v,z-\Delta z} + \frac{1}{h_{fg}}\left[\frac{q_{channel,z}\ \Delta z\ W_{channel}}{\dot{m}} - C_p\left(T_{sat} - T_{f,z}\right)\right] \tag{9}$$

$q_{channel}$ is the local heat flux, $W_{channel}$ is the channel width, T_{sat} is the saturation temperature, $T_{f,z}$ is local fluid temperature, C_p is the specific heat capacity, $\dot{m}$ is the mass flow rate given by:

$$\dot{m} = G\frac{H_{channel}W_{channel}}{N_{channel}} \tag{10}$$

G is the total mass flux, $H_{channel}$ is the channel height, $W_{channel}$ is the channel width, and $N_{channel}$ is the channels number.

4. RESULTS AND DISCUSSIONS

4.1. Comparison of the local measurement results with the predictions

4.1.1. Local heat transfer coefficients: comparison with correlations

As the channel size becomes small, the Reynolds number also becomes low for each tested mass flux. Therefore, measuring local heat transfer coefficient at low Reynolds number should be investigated for convective nucleate boiling. Figure 6 shows an example of the wall temperatures measured for the first channel at different locations along the flow direction. These temperatures are measured at steady state with microthermocouples located at 0.5 and 8.5 mm below the heat transfer surface. The inlet temperature of the water is kept at 64°C during all measurements. The total electrical power supplied to the heated plate is held constant at 200W. The results in figure 6 are presented for two different inlet mass fluxes 217 kg/m²s and 516kg/m²s. Figure 6 shows that the wall temperatures are lower at the channel inlet compared to wall temperature measured at channel outlet. The variation in the wall temperature at 0.5 and 8.5 mm below the heat exchange surface are comparable. The axial variation of the wall temperatures has a strong dependence of the flow patterns along the flow direction. Visual observation revealed that for all the measurements conducted in this work, three zones are identified. The first one at low z where the two phase flow was constituted by the isolated bubbles (figure 7a). The nucleate boiling dominates in this zone and the void fraction is low. After this zone, the wall temperature increases because the bubbles coalescence occurs and mass vapor occupies the maximum part of the channel section (figure 7b). The third zone is identified at the upstream flow where the void fraction is high and a partial dry out occurs nearly to the channel outlet (figure 7c). Therefore, the wall temperature attains its maximum value and saturation sate. During tests, it is observed that vapor seems to stay in the channel outlet blocking the flow. This is confirmed by figure 6 which shows that the wall in the upstream flow becomes isotherm and uniform because the temperatures measured at 0.5 and 8.5 mm below the heat transfer surface have approximately the same values. It can be seen that the length of this zone depends strongly on the inlet mass flux. As shown in figure 6, the isothermal zone length is about 100mm for 217 kg/m²s and 40mm for 516kg/m²s. In fact, for the same power supply, the coalescence phenomenon and the produced vapor masses increase by decreasing the inlet mass flux in the channel.

All the wall temperature measurements presented in figure 6 are used to estimate the local heat flux ($q_{channel,z}$) and local surface temperature ($T_{s,z}$) along the flow direction. Local heat transfer coefficients are deduced from equation (3) with a maximum uncertainty of 8%. Figure 8a and 8b show local distributions of the surface temperature and heat transfer coefficient for two inlet flow rates 516 kg/m²s and 217 kg/m²s. The results show a strong dependence of the local heat transfer coefficients and surface temperatures on the mass flux and z

location. For the same z location, the heat transfer coefficient is higher and the surface temperature is lower for 516 kg/m²s than for 217 kg/m²s. For the same mass flux, the surface temperature is lower and the heat transfer coefficient is higher in the channel inlet compared to all zones of the heat exchange surface along the channel length. In the channel inlet, nucleate boiling dominates and disturbance due to bubbles growing and escaping from the heat transfer surface contributes significantly to increase local heat transfer coefficient and decrease local surface temperature. Near the channel outlet, the heat transfer coefficient is deteriorated and surface temperature increases because the vapor covers a major part near the channel exit and prevents the liquid to wet the heat exchange surface. In this zone the mechanism of dry out contributes strongly to decrease the local heat transfer coefficient because it is visually observed during tests that vapor seems to be stay in the upstream flow and blocks the flow. This can be confirmed by estimating local vapor quality along the channel length. Figure 8c shows the local vapor quality for two different inlet mass flux 217 and 516kg/m²s. The experimental results in this figure are deduced from the results of local heat flux determined inversely. The local vapor quality is seen to increase along the channel length and with decreasing the mass flux. The curves presented in figure 8 show that both tests follow the same trend and the maximum vapor quality occurs at a z location depending on the mass flux.

There are more widely used correlations in the literature for predicting local heat transfer coefficient for flow boiling inside a channel. The major developed correlations define local Nusselt number ($Nu_z=h_zD_h/\lambda_L$) as a function of the Boiling number, vapor quality, and convection number. In figures 9a and 9b, the experimental measurements of local heat transfer coefficient are compared to the predictions of Kandlikar and Balasubramanian [32], Lazrek & Black [33], Warrier et al. [34], and Liu & Witerton [35].

Kandlikar and Balasubramanian [32] showed that for low Reynolds number, the nucleate boiling is the dominant flow mechanism. They recommended the following correlation by taking into account the presence of both nucleate boiling and convective boiling terms.

$$Nu_z = Nu_{Lo}\left(0.6683\,Co^{-0.2}\,f(Fr_{Lo}) + 1058\,Bo^{0.7}\right) \tag{11}$$

where Nu_{Lo} is the single phase Nusselt number assuming that all two phase flow as liquid. The function of the Froude number (Fr_{Lo}) is equal to 1 for two-phase flow in microchannels because there is no stratified flow. Co is the convection number given by:

$$Co = \left(\frac{1-x_{v,z}}{x_{v,z}}\right)^{0.8}\left(\frac{\rho_L}{\rho_v}\right)^{0.5} \tag{12}$$

$x_{v,z}$ is the local vapor quality, λ_L is the thermal condictivity, ρ_L and ρ_v are the liquid and vapor densities.

Lazarek & Black [33] are developed a correlation for local Nusselt number for flow boiling as a function of Boiling and liquid Reynolds numbers:

$$Nu_z = 30\, Re_{D_h}^{0.857}\, Bo^{0.714} \tag{13}$$

where Re_{D_h} is the liquid Reynolds number and Bo is the boiling number that defined by :

$$Re_{D_h} = \frac{G D_h}{\mu_L} \tag{14}$$

$$Bo = \frac{q_{channel,z}}{G h_{fg}} \tag{15}$$

G is the total mass flux, μ_L is the liquid viscosity, h_{fg} is the latent heat of vaporization, D_h is the hydraulic diameter:

$$D_h = 2\frac{H_{channel} W_{channel}}{H_{channel} + W_{channel}} \tag{16}$$

$H_{channel}$ is the channel height and $W_{channel}$ is the channel width.

Warrier et al. [34] proposed a correlation for local heat transfer for nucleate boiling inside a five parallel microchannels with a hydraulic diameter of 750 µm:

$$Nu_z = Nu_{Lo}\left(1 + 6\, Bo^{1/16} - 5.3(1 - 855\, Bo)\ \ x_{v,z}^{\ 0.65}\right) \tag{17}$$

Liu and Witerton [35] expressed local Nusselt number by introducing the enhancement factor due to the forced convective heat transfer mechanism due to the bubbles generation in the boundary layer next to the heat exchange surface.

$$Nu_z = \frac{D_h}{\lambda_L}\sqrt{(F\, h_{Lo})^2 + (S\, h_{pool})^2} \tag{18}$$

where h_{Lo} is the single phase heat transfer coefficient, h_{pool} is the pool boiling heat transfer coefficient defined by Copper [36], F is the forced convection enhancement factor, and S is the nucleate boiling suppression factor given by:

$$F = 0.35\ \left[1 + x_{v,z}\ \ \frac{\mu_L C_{p,L}}{\lambda_L}\ \ \left(\frac{\rho_L}{\rho_v} - 1\right)\right] \tag{19}$$

$$S = \left[1 + 0.055\, F^{0.5}\, Re_{D_h}^{0.16}\right] \tag{20}$$

Figures 9a and 9b show a comparison of the local heat transfer coefficients obtained with the various correlations listed above. It is shown that the correlation of Warrier et al. [34] predicted local heat transfer coefficient with a peak at approximately 35% vapor quality. The local heat transfer coefficient increases with vapor quality near the channel. Its maximum occurs at a vapor quality about 35%. After this value, the increase of the vapor quality decreases the local heat transfer coefficient predicted by Warrier et al. [34]. Lin et al. [37] and Bertsh et al. [38] found a similar shape of heat transfer coefficient versus vapor quality with a peak at low vapor quality. However, the correlations of Kandlikar and Balasubramanian [32], Lazrek & Black [33], and Liu & Witerton [35] predicted a monotonical decrease in local heat transfer coefficient with increasing vapor quality. Measurement results have the same trend accurately. For both mass fluxes, the local heat transfer coefficient is seen to decrease with increasing local vapor quality along the channel length. At low vapor quality, high nucleate boiling combined to the convective effect dominate and contribute to increase the local heat transfer. After this zone, the vapor quality increases because of the bubbles coalescence mechanism and therefore, bubbles frequency decreases. This explaines why the heat transfer decreases with increasing vapor quality. It is shown from figures 9a and 9b that the experimental results are closed with the Kandlikar and Balasubramanian [32] predictions. As shown in figure 9a, the local heat transfer coefficient becomes independent on the vapor quality when the vapor qualities is high as 80%. For high mass flux (figure 9b), the local heat transfer coefficient has a high variation with the vapor quality compared to the results obtained for low mass flux in figure 9a.

4.1.2. Local pressure drop: comparison of experiments and predictions

The tow phase pressure drop is defined as the sum of two components: frictional and momentum pressure drop. A large number of studies and available correlations are proposed for evaluating the fritional and momentum or accelerational pressure drop. The widely proposed correlations for microscale channels are used to estimate local pressure drop along the microchannel length and for comparison with the experimental measurement results. The aim of this section is to predict local pressure drop as a function of local vapor quality and to compare the total pressure measurements with predictions.

The momentum pressure drop reflects the increase of the kinetic energy of the flow during boiling process. It is dependent on the local vapor quality and local void fraction. The momentum pressure drop is given by [39]:

$$\Delta P_{m,z} = G^2 \left\{ \left[\frac{(1-x_{v,z})^2}{\rho_L (1-\alpha_z)} + \frac{x_{v,z}^{\ 2}}{\rho_v \alpha_z} \right]_{out} - \left[\frac{(1-x_{v,z})^2}{\rho_L (1-\alpha_z)} + \frac{x_{v,z}^{\ 2}}{\rho_v \alpha_z} \right]_{in} \right\} \quad (21)$$

where α_z is the void fraction calculated with the Rouhani and Axelson model [40], separated flow, and Wallis [42] equation. Rouhani and Axelson [40] proposed the following expression:

$$\alpha_z = \frac{x_{v,z}}{\rho_v} \left\{ \left[1 + 0.2\ (1-x_{v,z}) \left(\frac{g D_h \rho_L^{\ 2}}{G^2} \right)^{0.25} \right] \left(\frac{x_{v,z}}{\rho_v} + \frac{1-x_{v,z}}{\rho_L} \right) + \frac{1.18\ (1-x_{v,z})\ [g\sigma(\rho_L - \rho_v)]^{0.25}}{G \rho_L^{\ 0.25}} \right\}^{-1} \quad (22)$$

For separated flow model [41], each stream is assumed to travel at its own mean velocity. The void fraction is then defined as follows:

$$\alpha_z = \frac{1}{1 + \left(\frac{1-x_{v,z}}{x_{v,z}} \right) \frac{\rho_v}{\rho_L}} \quad (23)$$

Wallis [42] proposed an expression of void fraction as a function of Lockart-Martinelli [43] parameter χ as follows:

$$\alpha_z = \frac{1}{1 + 0.28\, \chi^{0.71}} \quad (24)$$

According to the separated flow model, the frictional pressure gradient of two-phase flow is calculated using the Lockart Martinelli parameters χ and ϕ defined by the following expressions:

$$\phi_L^{\ 2} = \frac{(dP/dz)_{TP}}{(dP/dz)_L} \quad (25)$$

where $(dP/dz)_{TP}$ is the two-phase frictional pressure gradient and $(dP/dz)_L$ is the single phase liquid pressure given by :

$$\left(\frac{dP}{dz} \right)_L = 2 \frac{f_L}{D_h} \frac{G^2 \left(1 - x_{v,z}^{\ 2}\right)}{\rho_L} \quad (26)$$

where f_L is the friction coefficient given by:

$$f_L = A\, Re_L^{\ -n} \quad (27)$$

For laminar flow A=16 and n=1 and for turbulent flow A=0.046 and n=0.2, Re_L represents the all-liquid Reynolds number calculated by:

$$Re_L = \frac{G D_h}{\mu_L} \quad (28)$$

The two phase friction multiplier ϕ can be given by:

$$\phi^2 = 1 + \frac{C}{\chi} + \frac{1}{\chi^2} \tag{29}$$

where C depends on the flow patterns of each phase. The Martinelli parameter χ is given by:

$$\chi = \left(\frac{\mu_L}{\mu_v}\right)^{0.1} \left(\frac{\rho_v}{\rho_L}\right)^{0.5} \left(\frac{1-x_v}{x_v}\right)^{0.1} \tag{30}$$

The parameter C varies from 5 to 20 as proposed by Ghislom [44]. For laminar flow C=5 for macrochannel. Mishima and Hibiki [45] used the Ghislom correlation to predict pressure drop for small channels ranging in diameter from 1.05 to 3.90mm. They introduced the effect of hydraulic diameter on the coefficient C. English and Kandlikar [46] modified the Mishima and Hibiki correlation and proposed the following expression for laminar liquid and vapor flows:

$$C = 5\left(1 - e^{-319 D_h}\right) \tag{31}$$

Lee and Lee [47] proposed the following empirical correlation for calculating C:

$$C = 6.83310^{-8} \left(\frac{\mu_L{}^2}{\rho_L \sigma D_h}\right)^{-1.317} \left(\frac{G\mu_L}{\sigma}\left(\frac{x_v}{\rho_v} + \frac{1-x_v}{\rho_L}\right)\right)^{0.719} Re_L{}^{0.557} \tag{32}$$

where σ is the surface tension.

Lee an Mudawar [48] measured two-phase pressure drops for evaporation of water in multimicrochannels. They proposed the following expression for laminar vapor and liquid flows:

$$C = 2.16\ Re_L{}^{0.047} \left(\frac{G^2 D_h}{\sigma \rho_L}\right)^{0.6} \tag{33}$$

Figure 10 Compares momentum pressure calculated with eq (21). Local void fraction is calculated as a function of the local vapor quality using three models for comparison: the Rouhani and Axelson model [40], separated flow [41], and Wallis [42] model. Local vapor quality is deduced from the local heat flux and surface temperature. It is shown that all these correlations predicted the comparable values of momentum pressure.

Figure 11 presents the comparison of the frictional pressure drop obtained for inlet mass flux of 217 kg/m²s and 516kg/m²s using the correlation of English and Kandlikar [46], Lee and Lee [47] and Lee and Mudawar [48]. It is shown that all theses correlations give the comparable values of local frictional pressure. It can be seen that the local frictional pressure drop increases along the channel length and with local vapor quality.

The total pressure drop ($\Delta P_{t,z}$) is defined as the sum of the momentum ($\Delta P_{m,z}$) and the frictional pressure ($\Delta P_{f,z}$).

$$\Delta P_{t,z} = \Delta P_{m,z} + \Delta P_{f,z} \quad (34)$$

Figure 12 shows a comparison of the measured and predicted values of total pressure drop for G varying from 167 kg/m²s to 616 kg/m²s. It can be seen from this figure that the predicted values by the correlations of English & Kandlikar [46], Lee & Lee [47], and Lee & Mudawar [48] agree reasonably well with the experimental data. All these correlations are based on combination of laminar liquid and laminar vapor flows and also account the effect of channel size and section geometry on the pressure drop. It can be noted that in all the correlation's pressure drop, the vapor quality was determined locally from the local heat flux and local surface temperature that estimated from IHCP. This is probably the reason that why the correlations of English & Kandlikar [46], Lee & Lee [47], and Lee & Mudawar [48] give the better prediction of the total pressure drop close to the measurements results.

4.2. Local heat transfer and pressure drop for convective boiling of nanofluids

4.2.1. Preparation of nanofluid

In this work, some experiments are conducted using nanofluid (Cu nanoparticles-suspension) as the working fluid. The de-ionized water is used as the base fluid. The copper nanoparticles which average diameter is about 35 nm are dispersed in the de-ionized water. The ultrasonic vibration is used to stabilize the dispersion of the nanoparticles in the base fluid. In order to improve the nanoparticles uniformity in the water and to prevent their coagulation, the nanofluid has been vibrated during 24h by an ultrasonic processor. No surfactant was added in the water-nanoparticles suspension to stabilize the nanoparticles suspension. The reason for this is that the addition of the surfactant can influence the real enhancement of the boiling heat transfer using nanoparticles. During experiments, nanoparticles are maintained a good dispersion in the nanofluid. It was noticed that the nanoparticles suspension changes after four or five days.

In this paper, experiments on heat transfer of convective boiling are conducted using three different concentrations of nanoparticles : 5 mg/L, 10 mg/L and 50 mg/L. The measurements are compared with the results obtained using pure water. For different flow rate, the duration of all tests is about 12 h. After each experiment, the experimental section was cleaned with the de-ionized water. It is shown from the previous work

that the motion of the two-phase flow prevents nanoparticles deposition and variation of nanoparticles concentration [49, 50].

4.2.2. Effect of nanoparticles concentration on the local heat transfer coefficient

In this study, experiments were conducted with very low mass fraction of Cu nanoparticles. The reason is that for low nanoparticles concentration, nanoparticles deposition on the surface and variation of the nanoparticles concentration in the base fluid can be ignored. The mass fraction of the Cu nanoparticles is given by:

$$\mathrm{wt\%} = 100\frac{m_p}{m_p + m_w} \tag{35}$$

where m_p is the copper nanoparticles mass, and m_w is the de-ionized water mass.

The volume fraction of nanoparticles is given by:

$$\phi = \frac{\mathrm{wt}\,\rho_w}{\mathrm{wt}\,\rho_w + (1-\mathrm{wt})\rho_p} \tag{36}$$

where ρ_w is the water density, and ρ_p is the Cu nanoparticles density.

Figure 13 shows the wall temperatures measured at steady state with microthermocouples placed at 0.5 mm below the heat exchange surface. The results obtained in this figure are obtained for the following operating conditions : the electrical power input is of 200W, the inlet liquid temperature is of 64°C, and the mass flux is of 516kg/m²s. Tests are made for three different volume fractions of nanoparticles in the base fluid: 5 mg/L ($\phi = 0.00056\%$), 10 mg/L ($\phi = 0.0011\%$) and 50 mg/L ($\phi = 0.0056\%$). It can be noticed that the wall temperature decreases by increasing the nanoparticles concentration. Near the channel inlet, the wall temperature is reduced from 86.5 for boiling of pure water to 83°C for boiling of nanofluid with 50 mg/l of Cu concentration. Near the channel outlet, saturation temperature is of 100°C for boiling of pure water and it is decreased to 98°C for boiling of nanofluid with 50 mg/l of Cu concentration. It can be concluded that nanoparticles concentration in the base fluid reduces the boiling temperature because the copper nanoparticles contribute to increase heat transfer locally and accelerate incipient boiling.

Figure 14 shows the effect of copper nanoparticles concentration on the enhancement of the local heat transfer coefficients estimated inversely using the experimental data presented in figure 13. It is shown that the heat transfer coefficient enhancement increases with the Cu nanoparticles concentration. Figures 15 and 16 show respectively the surface temperatures and the local heat flux estimated inversely for different Cu nano-particles

concentrations. It can be noted that the non-uniform profile of the heat flux along the flow direction can be due to the mechanism of the bubbles departure and agitation after their detachment from the nucleation sites and the induced liquid convection. The best case corresponds to the maximum heat transfer coefficient and the minimum surface temperature and it is obtained for high copper nanoparticles concentration. The present results show that the local heat transfer coefficient increases with the copper nanoparticles concentration not only because the difference between the surface and the inlet liquid temperature decreases but also because the local heat flux at the boiling surface increases. In the previous work [51], it is noted that the heat transfer of nanofluid should much better than that of pure water because the thermal conductivity increases with the nanoparticles concentration. Kim et al. [20] showed that departing bubbles size increases and bubbles frequency decreases using nanofluid. You et al. [52] investigated an experimental study to find the boiling curve in pool boiling from a flat square heater immersed in Al_2O_3-water nanofluid. They found no degradation or enhancement nucleate boiling heat transfer. In the present work, the experimental results confirms that for forced convective boiling not only the local heat transfer coefficient increases but also the local heat flux, but the local surface temperature decreases with nanoparticles suspension in de-ionized water. The reason is due probably to the flow velocity because as the flow velocity increases, the drag force induces the departure bubbles at small diameter and increases nanoparticles migration in base fluid.

4.2.3. Effect of nanoparticles concentration on the local pressure drop

In the previous work, it is noted that the presence of nanoparticles in the de-ionized water can increase pressure drop in microchannels because the dynamic viscosity increases with nanoparticles concentration. Some authors [53] measured the inlet and outlet pressure drop for single phase in microchannels and confirmed that pressure drop increases with Reynolds number and nanoparticles concentration. In this paper, the measurement of pressure drops is made at the inlet and outlet of the parallel channels. The local pressure drop is determined from the experimental results such as the local vapor quality and surface temperatures as shown in the previous sections. The surface temperatures and nanoparticles concentration are used to determine the physical properties of base fluid (water) and nanofluid. Figure 17 shows the variation of the local pressure drop for water and different nanoparticles-water suspensions. The local pressure drop for nanofluids are determined using equations 21 and 22 for calculating frictional pressure and equations 25 to 31 for calculating momentum pressure including nanofluid properties that defined as follows:

$$h_{fg,n} = \frac{\rho_w}{\rho_p}(1-\phi)h_{fg,w} \tag{37}$$

$$\rho_n = (1-\phi)\rho_w + \phi\rho_p \quad (38)$$

$$\mu_n = \mu_w(1-\phi)^{-2.5} \quad (39)$$

The measurement results presented in figure 17 are obtained for the power supply of 200W, inlet liquid temperature of 64°C, mass flux of 516 kg/m²s. It is shown that for the same vapor quality, local pressure drop is higher for Cu-water nanofluid than for pure water and it increases with nanoparticles concentration because viscosity is high for Cu-water nanofluid than for pure water viscosity. Figure 18 compares local vapor quality for each tested fluid. It is shown that the vapor quality also increases with nanoparticles concentration because the local heat flux increases with Cu nanoparticles suspension.

CONCLUSIONS

An experimental study of forced convective boiling of pure water and copper-water nanofluids in vertical microchannels has been conducted and the major conclusions are retained. This work treated forced convective boiling heat transfer by combining two advantages such as microchannels and nanofluids. The nanofluid with extremely low concentration nanoparticles was used to enhance the boiling heat transfer. In this paper, the principal experimental results on local heat transfer of nanofluid containing different small copper nanoparticles are presented. The pressure drop and local surface temperature of nanofluid are also investigated. Inverse heat conduction procedure is successfully applied to estimate the local thermal boundaries conditions. The local heat transfer coefficients measured for pure water are close to those predicted by Kandlikar and Balasubramanian [32]. The Cu-water nanofluid shows higher local heat transfer coefficient, higher local heat flux, higher pressure drop, and lower surface temperature than its base fluid at the same mass flux. Vapor quality has been shown locally to be dependent on the Cu nanoparticles concentration in nanofluid. The increase in the heat transfer and pressure drop of Cu-water nanofluid is mainly due to its high viscosity compared to the base fluid. The present results are somewhat contrary to some previous results obtained on pool boiling heat transfer where the addition of the nanoparticles into the base fluids did not enhance heat transfer and causes no significant improvement in pressure drop. In this paper, it is revealed that Cu-water nanofluid is very suitable for cooling microsystems using forced convective boiling nanofluid with the small concentrations.

NOMENCLATURE

C_p	specific heat capacity, J/kg K
D_h	hydraulic diameter, m
E	thickness, m
$H_{channel}$	channel height, m
h	heat transfer coefficient, W/m^2K
L	channel length, m
q	heat flux, W/m^2
P	Pressure, Pa
T	temperature, K
$W_{channel}$	channel width, m.
z	axial coordinate, m

Greek symbols

λ	thermal conductivity, W/mK
μ	dynamic viscosity, kg/ms
ρ	density, kg/m^3

Subscript

f	frictional
in	inlet
m	momentum
n	nanofluid
out	outlet
p	nanoparticles
s	surface
t	total
w	water
z	local value

REFERENCES

[1] J.R. Thome, Boiling in microchannels: a review of experiment and theory, International Journal of Heat and Mass Transfer, 25 (2004) 28-139.

[2] W. Qu, I. Mudawar, Transport phenomena in two-phase micro-channel heat sinks, Journal of Electronic Packaging, ASME, 126 (2004) 213-223.

[3] Y. Xuan, Li Qiang, Heat Transfer Enhancement of nanofluids. International Journal of Heat and Fluid Flow. 21 (2000) 58-64.

[4] S.G. Kandlikar, P. Balasubramanian, An extension of the flow boiling correlation to transition laminar and deep laminar flows in minichannels and microchannels, Heat Transfer Engineering, 25(3) (2004) 86–93.

[5] J.R. Thome, V. Dupont, A.M. Jacob, Heat transfer model for evaporation in microchannels. Part I: presentation of the model, International Journal of Heat and Mass Transfer, 47 (2004) 3375–3385.

[6] Y. Yang, Z. George, B. Zhang, A. Eric, A. Grulke, B. William, B. Anderson, B. Gefei Wu, Heat transfer properties of nanoparticle-in-fluid dispersions (nanofluids) in laminar flow, International Journal of Heat and Mass Transfer, 48 (2005) 1107–1116.

[7] S.G. Kandlikar, Heat transfer mechanisms during flow boiling in microchannels, J. of Heat Transfer, ASME, 126 (2004) 8-16.

[8] S. Lee, S.U.S. Choi, S. Li, J.A. Eastman, Measuring thermal conductivity of fluids containing oxide nanoparticles, J. Heat Transfer, 121 (1999) 280–289.

[9] S. Maïga, S.J. Palm, C.T. Nguyen, G. Roy, N. Galanis, Heat transfer enhancement by using nanofluids in forced convection flows, International Journal of Heat and Fluid Flow, 26 (2005) 530–546.

[10] X. Wang, X. Xu, S.U.S. Choi, Thermal conductivity of nanoparticle-fluid mixture, J. Thermophys. Heat Transfer 13 (4) (1999) 474–480.

[11] Y. Xuan, W. Roetzel, Conceptions for heat transfer correlations of nanofluids, Int. J. Heat Mass Transfer 43 (2000) 3701–3707.

[12].J.A. Eastman, SUS Choi, S. Li, W. Yu, L.J. Thomson, Anomalously increased effective thermal conductivities of ethylene glycol-based nanofluids containing copper nanoparticles, Appl. Phys. Lett. 78 (2001) 718-200.

[13] S.M.S. Murshed, K.C. Leong, C. Yang, Enhanced thermal conductivity of TiO2 - water based nanofluids, International Journal of Thermal Sciences, 44 (2005) 367-373.

[14] T.K. Hong, H.S. Yang, C.J. Choi, Study of the enhanced thermal conductivity of Fe nanofluids, J. Appl. Phys., 97 (2005) 64-311.

[15] J. Buongiorno, Convective transport in nanofluids, J. of Heat Transfer, Transaction ASME, 128 (2006) 240-250.

[16] C.T. Nguyen, G. Roy, Ch. Gauthier, N. Galanis, Heat transfer enhancement using Al2O3 –water nanofluid for an electronic liquid cooling system, Applied Thermal Engineering, 27 (2007) 1501-1506.

[17] S. Zeinali Heris, M. Nasr Esfahany, S.G. Etermad, Experimental investigation of convective heat transfer of Al2O3/water nanofluid in circular tube, Int. J. Heat and Mass Transfer, 28(2) (2007) 203-210.

[18] S. Lee, S.U.S. Choi, S. Li, J.A. Eastman, Measuring thermal conductivity of fluids containing oxide nanoparticles, ASME Journal of Heat Transfer, 121(2) (1999) 280-289.

[19] S.J. Kim, I.C. Bang, J. Buongiorno, L.W. Hu, Study of pool boilng and critical heat fluw enhancement in nanofluids, Bulletin of the Polish Academy of Sciences, Technical sSiences, 55 (2) (2007) 211-216.

[20] Y. He, H. Jin, Y. Chen, D. Ding, H. Cang, H. Lu, Heat transfer and flow behaviour of aqueous suspensions of TiO2 nanoparticles (nanofluids) flowing upward through a vertical pipe, Int. J. of Heat and Mass Transfer, 50 (2007) 2272-2281.

[21] Sh. Kang, W.Ch. Wei, Sh.H. Tsai, Sh.Y. Yang, Experimental investigation of silver nano-fluid on heat pipe thermal performance, Applied Thermal Engineering, 26 (2006) 2377-2382.

[22] P. Vassallo, R., Kumar, S. D'Amico, Pool Boiling Heat Transfer Experiments in Silica-Water Nano-Fluids. International Journal of Heat and Mass Transfer, 47 (2003), 407-411.

[23] S.M. You, J.H. Kim, K.H. Kim, Effect of nanoparticles on critical Heat Flux of Water in Pool Boiling Heat Transfer. Applied Physics Letters, 83 (2003) 3374-3376.

[24] Z.H. Liu, J.G. Xiong, R. Bao, Boiling heat transfer characteristics of nanofluis in a flat heat pipe evaporator with micro-grooved heating surface, Int. J. of Multiphase Flow, 33 (2007) 1284-1295.

[25] J. Lee, I. Mudawar, Assessement of the effectiveness of nanofluis for single-phase and two-phase heat transfer in micro-channels, Int. J. of Heat and Mass Transfer, 50 (2007) 452 463.

[26] J. H. Kim, K.H. Kim, S.M. You, Pool Boiling Heat Transfer in Saturated Nanofluids. Proceedings of ASME Int. Mech. Engineering Congress, Anaheim, California, 2004.

[27] V. Trisaksri, S. Wongwises, Nucleate pool boiling heat transfer of TiO2-R141b nanofluids, Int. J. of Heat and Mass Transfer, 52 (2009) 1582-1588.

[28] P. Cheng, H.Y. Wu, F.J. Hong, Phase-change heat transfer in microsystems, Journal of Heat Transfer, Transaction ASME, 129 (2007) 101-107.

[29] O.M. Alifanov, E.A. Artyukhin, S.V. Rumyantsev, Extreme methods for solving Ill-posed problems with applications to inverse heat transfer problems, Begell House, New York, 1995.

[30] H. Louahlia-Gualous, P.K. Panday, E.A. Artioukhine, Inverse determination of the local heat transfer coefficients of nucleate boiling on a horizontal cylinder, ASME Journal of Heat Transfer, 125 (2003) 1087-1095.

[31] Louahlia-Gualous H., L. El Omari, Local heat transfer for the evaporation of a laminar falling liquid film on a cylinder - Experimental, numerical and inverse heat conduction analysis, Numerical Heat Transfer, Part A: Applications, 50 (7) (2006) 667-688.

[32] S.G. Kandlikar, P. Balasubramanian, An extension of the flow boiling correlation to transition, laminar and deep laminar flows in minichannels and microchannels, Heat Transfer Eng., 25(3) (2004) 86–93.

[33] G.M. Lazarek, S.H. Black, Evaporative heat transfer, pressure drop and critical heat flux in a small vertical tube with R-113, Int. J. of Heat and Mass Transfer, 25 (1982) 945-960.

[34] G.R. Warrier, V.K. Dhir, L. A. Momoda, Heat Transfer and pressure drop in narrow rectangular channels, Exp. Therm and Fluid Science, 26 (2002) 53-64.

[35] Z. Liu, R.H.S. Witerton, A general correlation forsaturated and subcooled flow boiling in tubes and annuli, based nucleate pool boiling equation, Int. J. Heat and Mass Transfer, 34 (1991) 2759-2766.

[36] J. Collier, J. Thome, Convective boiling and condensation, third ed. Oxford University Press, Oxford, 1994.

[37] S. Lin, P.A. Kew, K. Cornowell, Two phase heat transfer to a refrigerant in a 1 mm diameter tube, Int. J. Refrig. 24 (2001) 51-56.

[38] S.S. Bertsch, E.A. Groll, S.V. Garimella, Refrigerant flow boiling heat transfer in parallel microchannels as a function of local vapor quality, Int. J. of Heat and Mass Transfer, 51 (2008) 4775-4787.

[39] J.M. Quibén, L. Cheng, R.J. da Silva Lima, J.R. Thome, Flow boiling in horizontal flattened tubes:Part I Two phase frictional pressure drop results and model, Int J. of Heat and Mass Transfer, 52 (2009) 3634-3644.

[40] Z. Rouhani, E. Axelsson, Calculation of volume void fraction in a subcooled and quality region, Int. J. Heat Transfer, 17 (1970) 383-393.

[41] J. Thome, Engineering data book III, chapter 13 1-34, 2004.

[42] G.B. Wallis, One-dimensional two-phase flow, Mc Graw-Hill, New York, 1969.

[43] R.W. Lockart Martinelli, proposed correlation of data for isothermal two phase two component flow in pipes, Chem. Eng Prog, 45 (1949) 39-48.

[44] D. Ghislom, Two-phase flow in pipelines and heat exchangers, Longman, New York, 1983.

[45] K. Mishima, T. Hibiki, Some characteristics of air water two-phase flow in small diameter vertical tubes, Int. J. Multiphase flow, 22 (1996) 1767-1778.

[46] N.J. English, S.G. Kandlikar, An experimental investigation into the effect of surfactants on air-water two phase flow in minichannels, Heat Transfer Engineering, 27 (2006) 99-109.

[47] H.J. Lee, S.Y. Lee, Heat transfer correlation for boiling flows in small rectangular horizontal channels with low aspect ratios, Int. J. Multiphase flow, 27 (2001) 2043-2062.

[48] H.J. Lee, I. Mudawar, Two-phase flow in high heat flux micro-channel heat sink for refrigeration cooling applications: Part II-heat transfer characteristics, Int. J. of Heat and Mass Transfer, 48 (2005) 941-955.

[49] S.K. Das, N. Putra, W. Roetzel, Pool boiling characteristics of nano-fluids. International Journal of Heat and Mass Transfer 46 (5) (2003) 851-862.

[50] Z.H. Liu, J.G. Xiong, R. Bao, Boiling heat transfer characteristics of nanofluids in a flat heat pipe evaporator with micro-grooved heating surface. International Journal of Multiphase Flow, 33 (2007) 1284-1295.

[51] V. Trisaksri, S. Wongwises, Critical review of heat transfer characteristics of nanofluids, Renewable and Sustainable Energy Reviews, 11 (2007) 512-523.

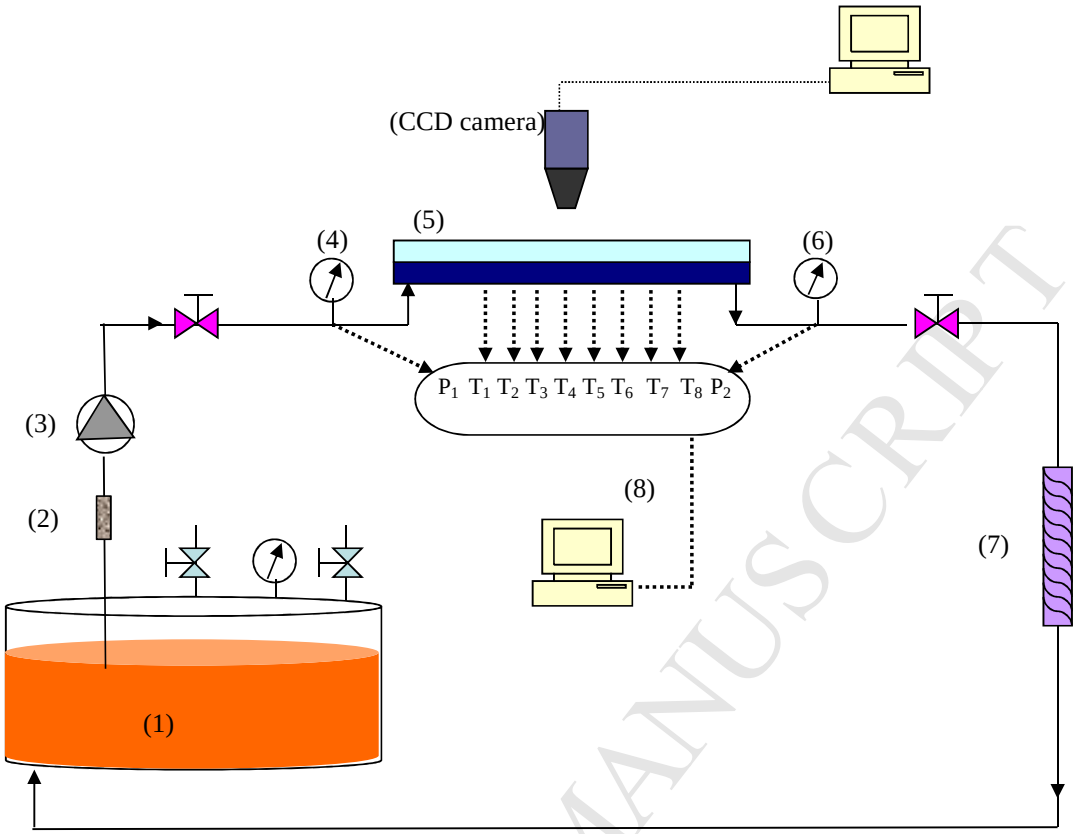

Figure 1. A schematic diagram of the test facility

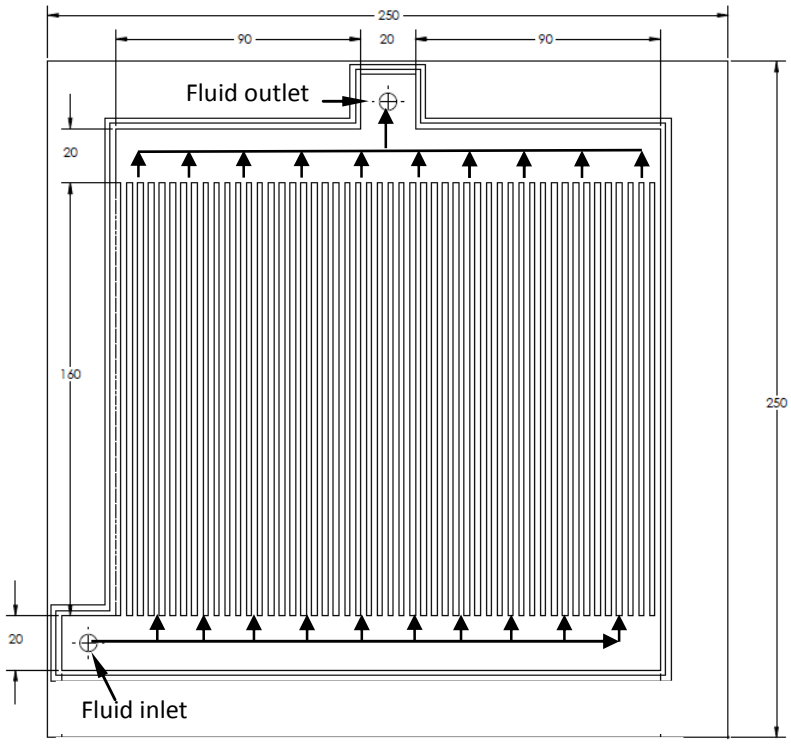

(a)

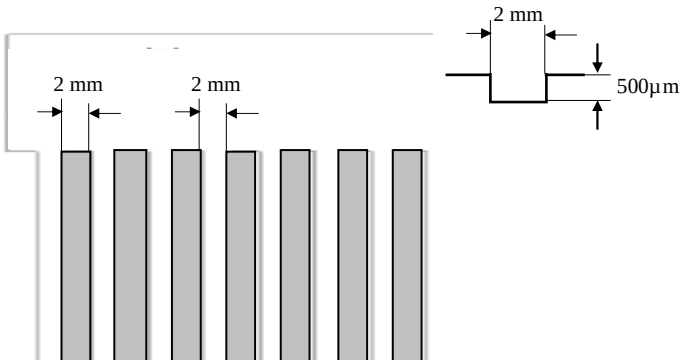

(b)

Figure 2. Minichannels test section: (a) the top view of minichannels heat sink, (b) construction of the minichannels in the test module.

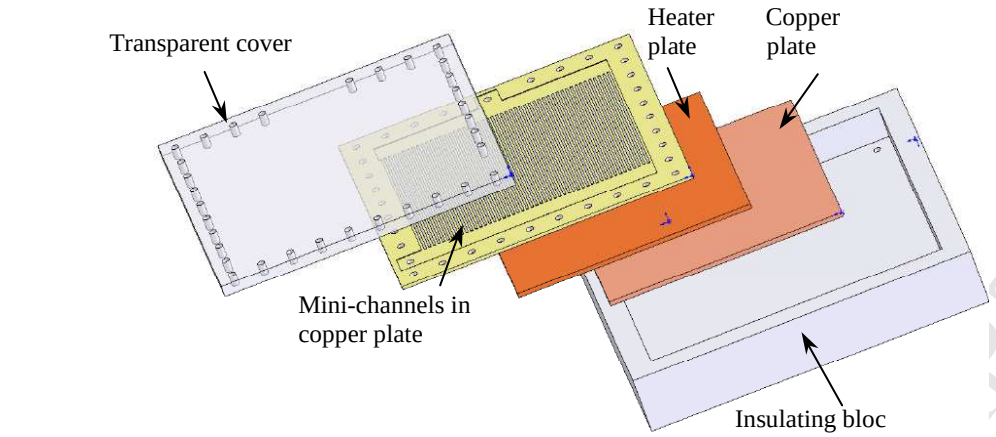

(a)

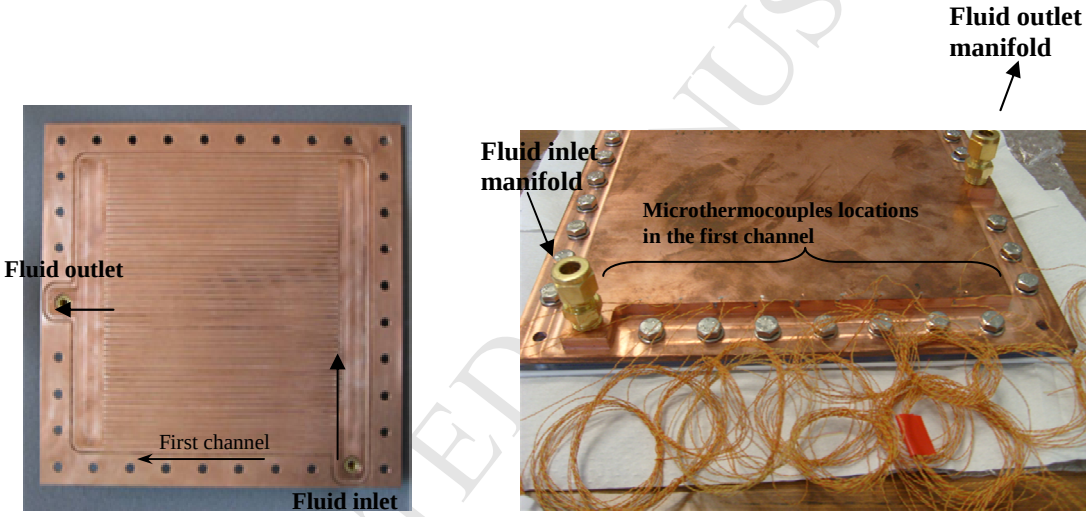

(b) (c)

Figure 3: (a) test module assembly, (b) top side of copper test plate, (c) bottom side of copper test plate.

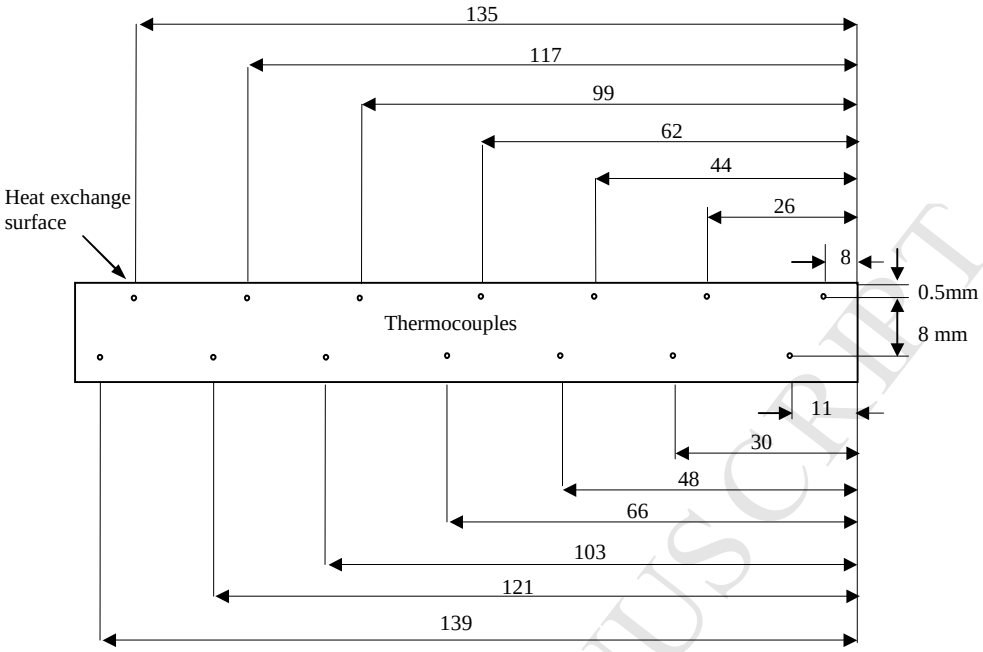

Figure 4. Thermocouple locations in the first minichannel

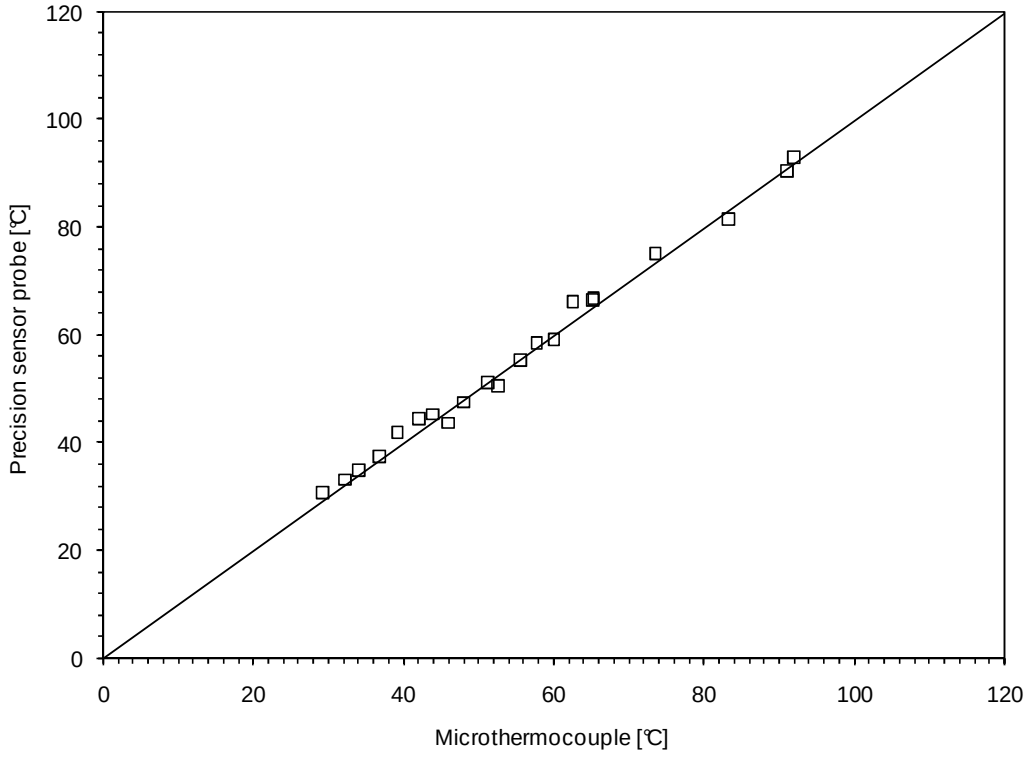

Figure 5: Example of microthermocouple calibration curve.

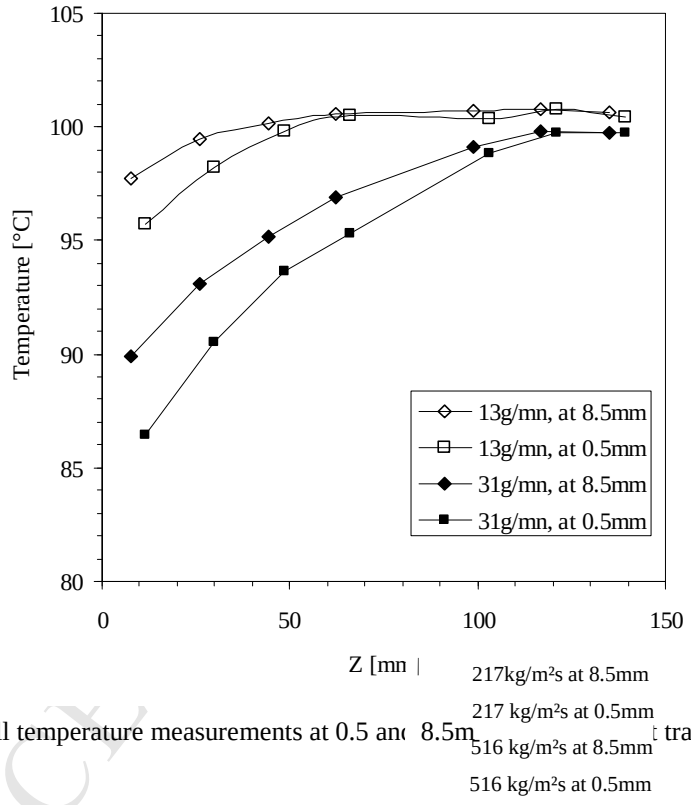

Figure 6. Wall temperature measurements at 0.5 and 8.5m t transfer surface.

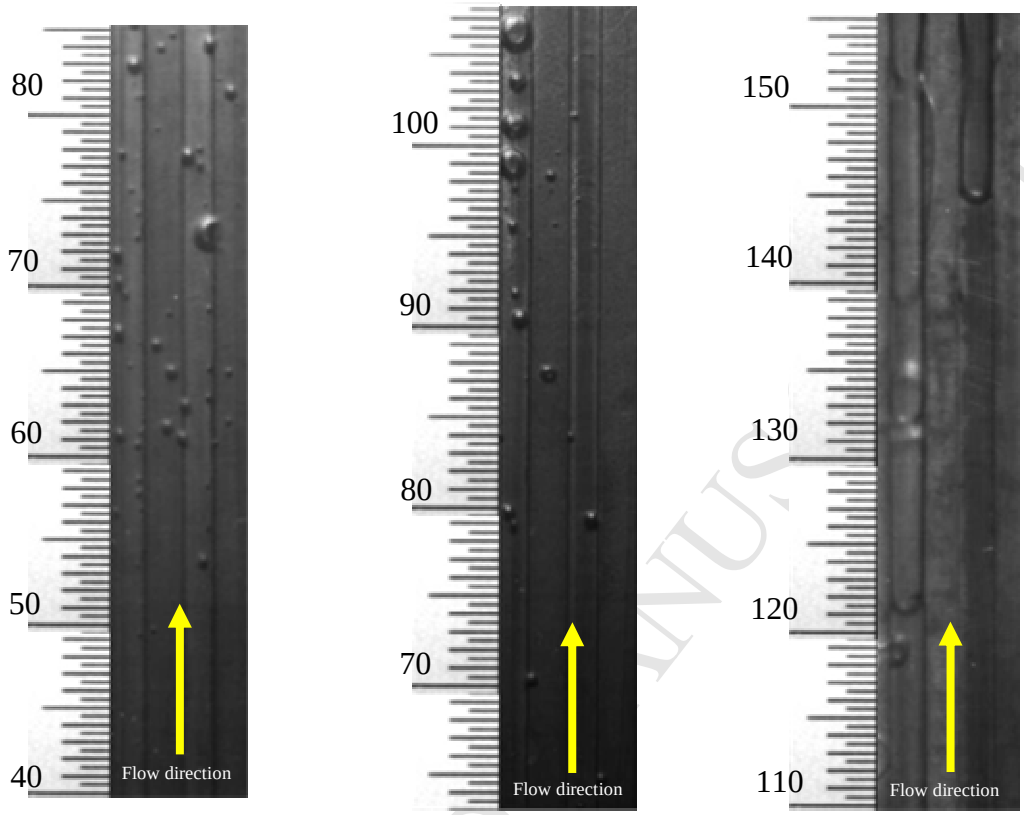

(a) (b) (c)

Figure 7. Boiling flow patterns along the channel length (a) $40mm \le z \le 85mm$. (b) $63mm \le z \le 107mm$, (c) $110mm \le z \le 155mm$

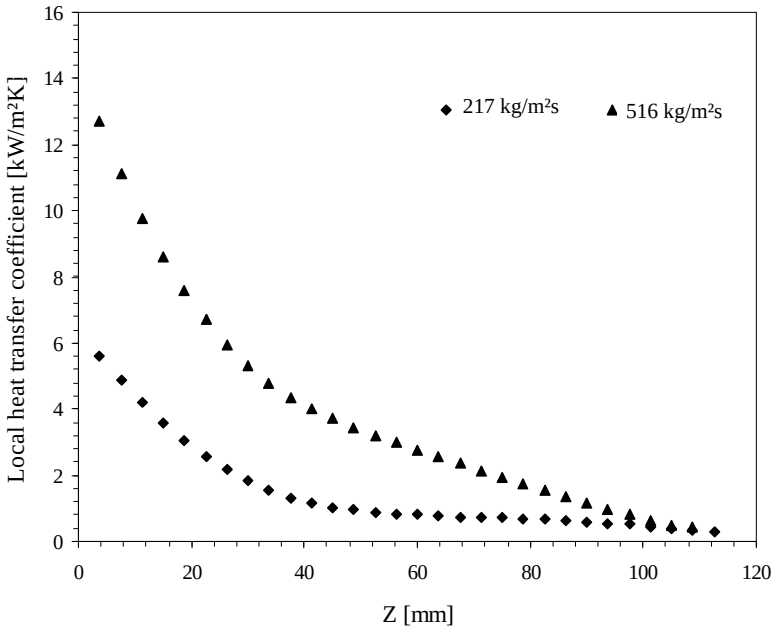

(a)

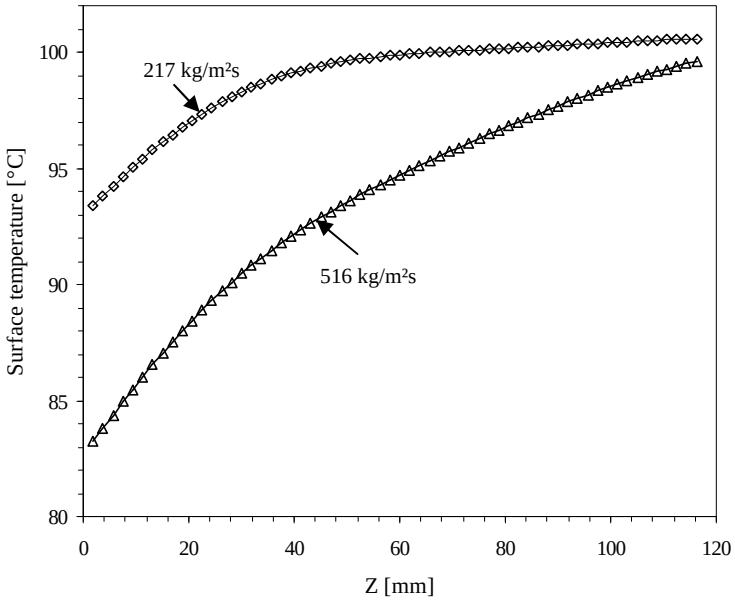

(b)

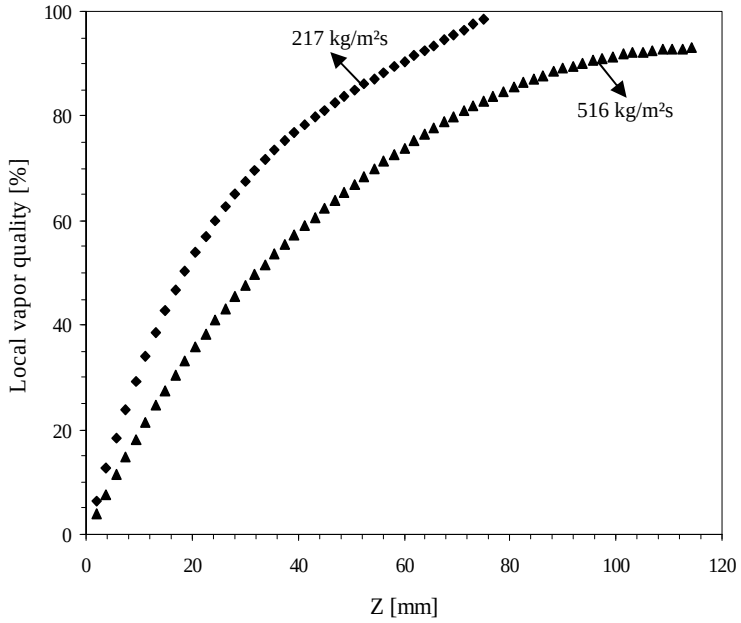

(c)

Figure 8: Local thermal parameters for 217 kg/m²s and 516kg/m²s: (a) heat transfer coefficient, (b) surface temperature, (c) vapor quality.

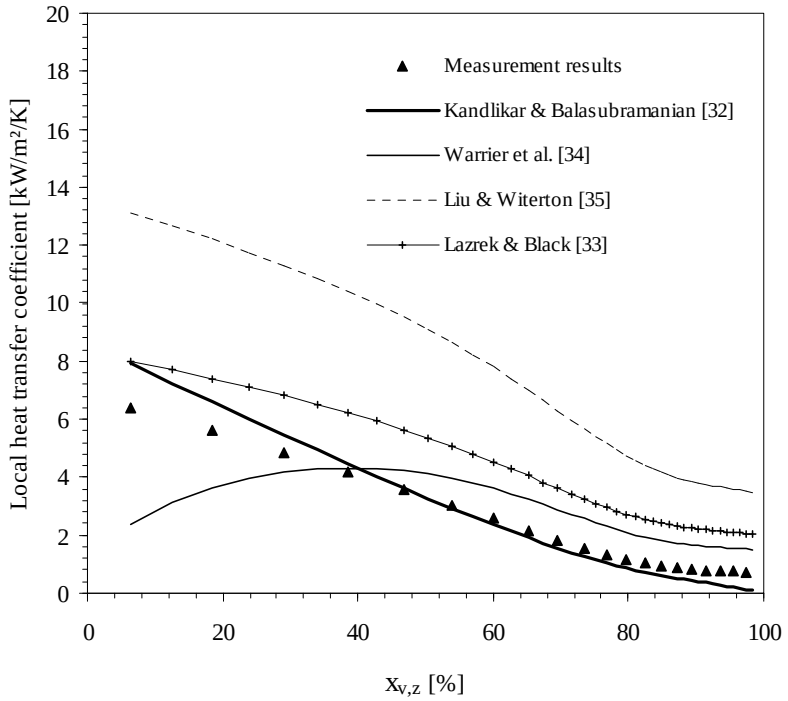

(a)

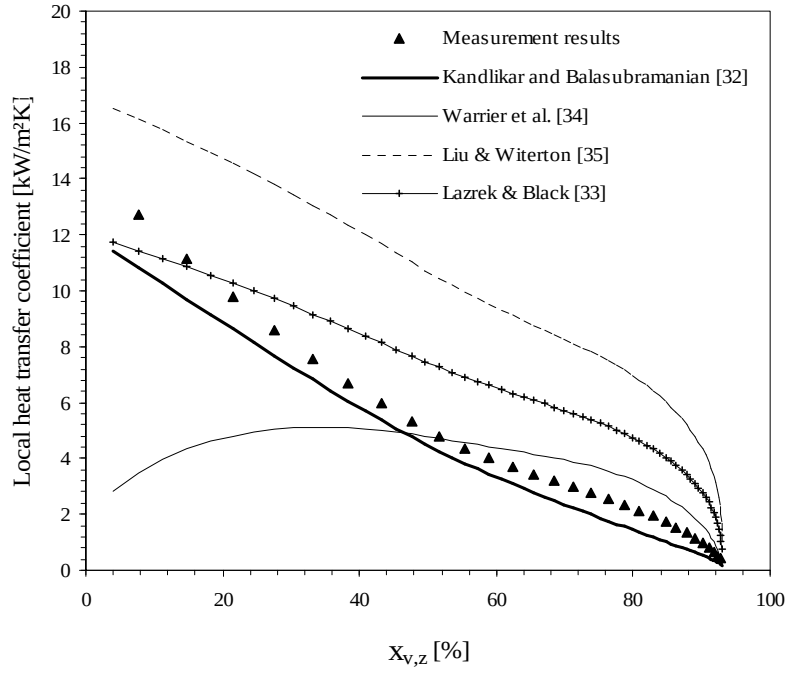

(b)

Figure 9. Comparison of measured and predicted local heat transfer coefficient for : (a) 217kg/m²s and (b) 516kg/m²s

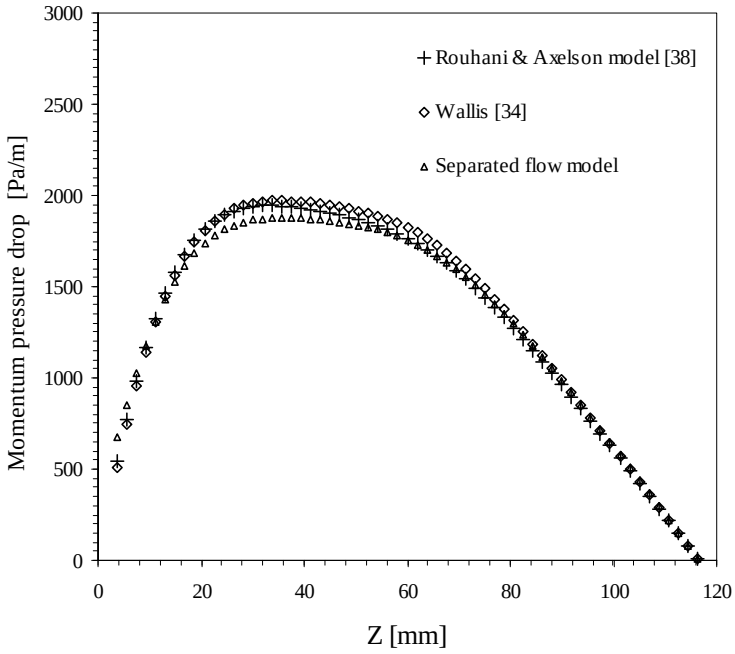

Figure 10. Comparison of local momentum pressure drop.

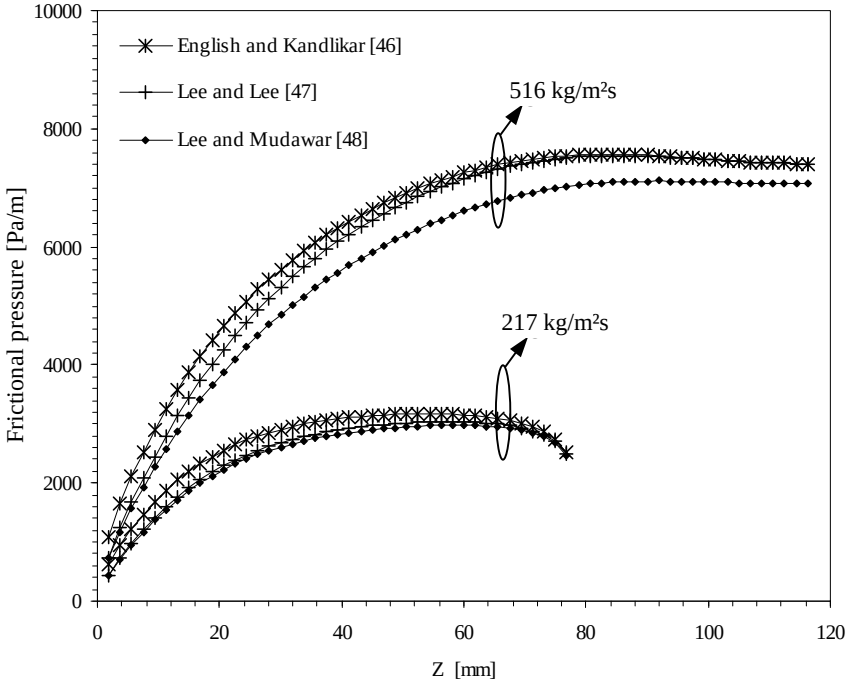

Figure 11. Comparison of local frictional pressure drop

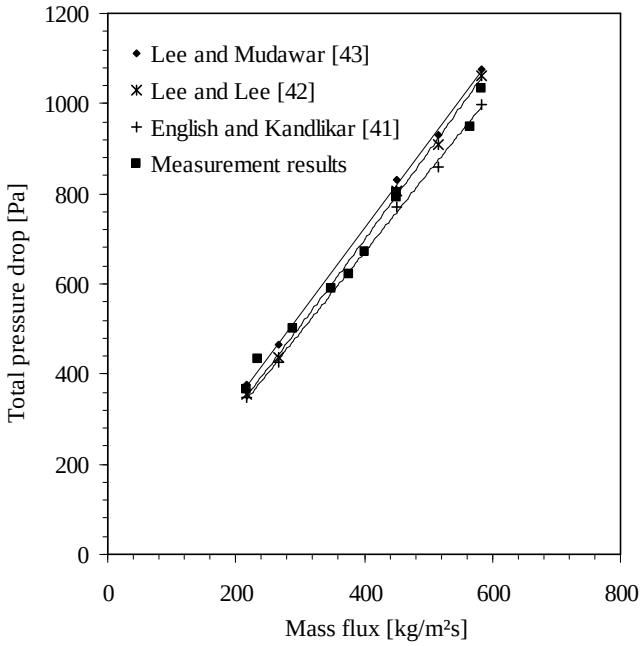

Figure 12: Comparison between predicted and measured total pressure drop.

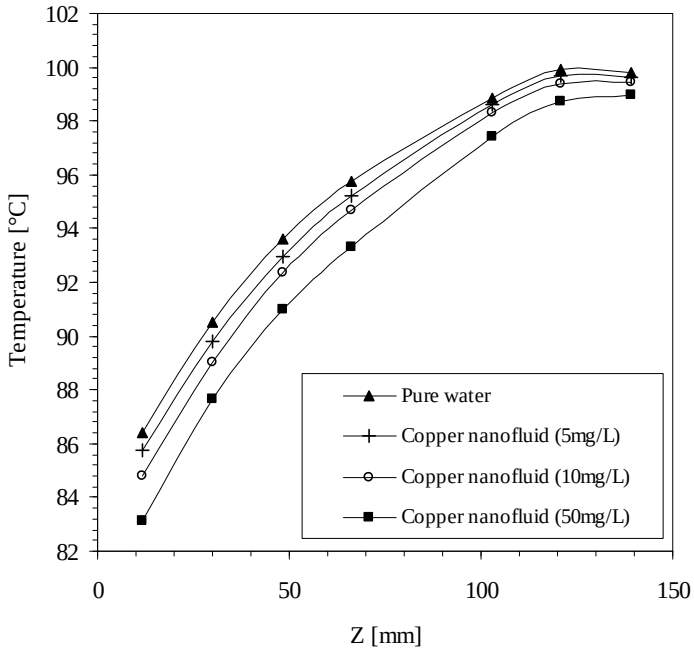

Figure 13. Wall temperatures measured at 0.5mm below the heat transfer surface.

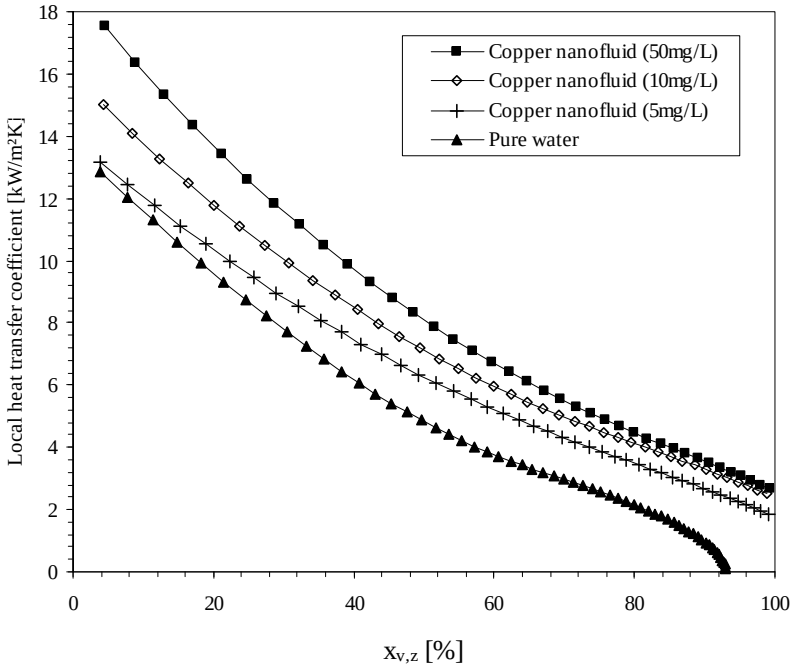

Figure 14. Effect of Cu nanoparticles concentration on local heat transfer coefficients.

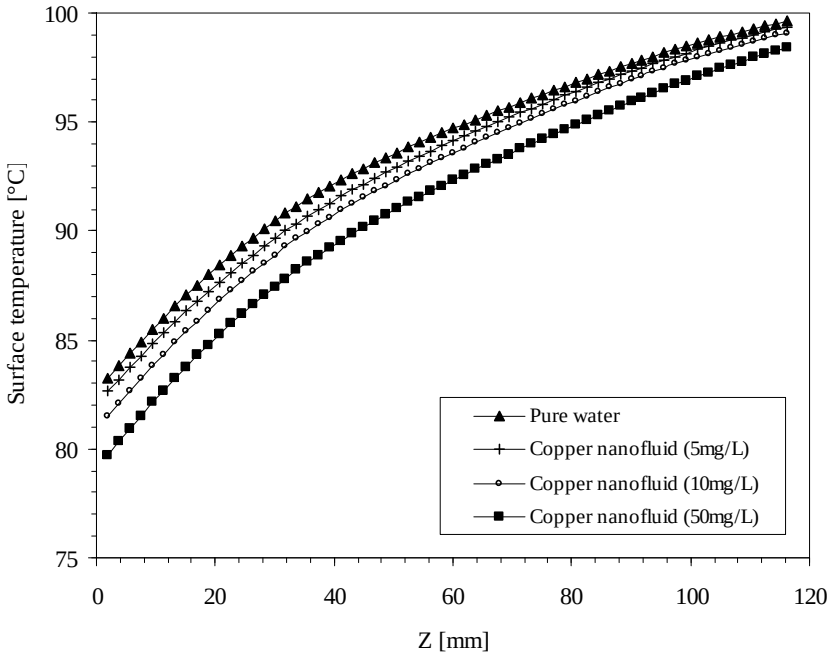

Figure 15. Effect of Cu nanoparticles concentration on local surface temperature.

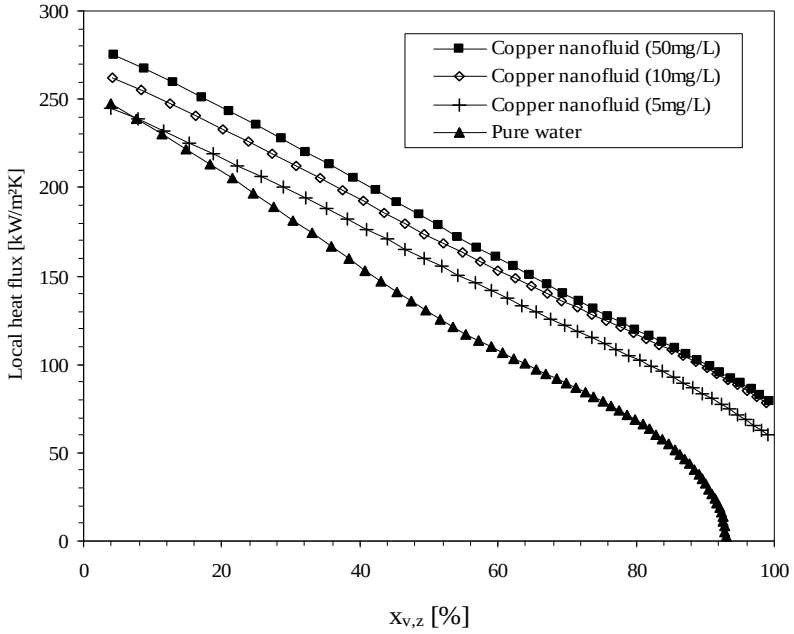

Figure 16. Effect of Cu nanoparticles concentration on local heat flux.

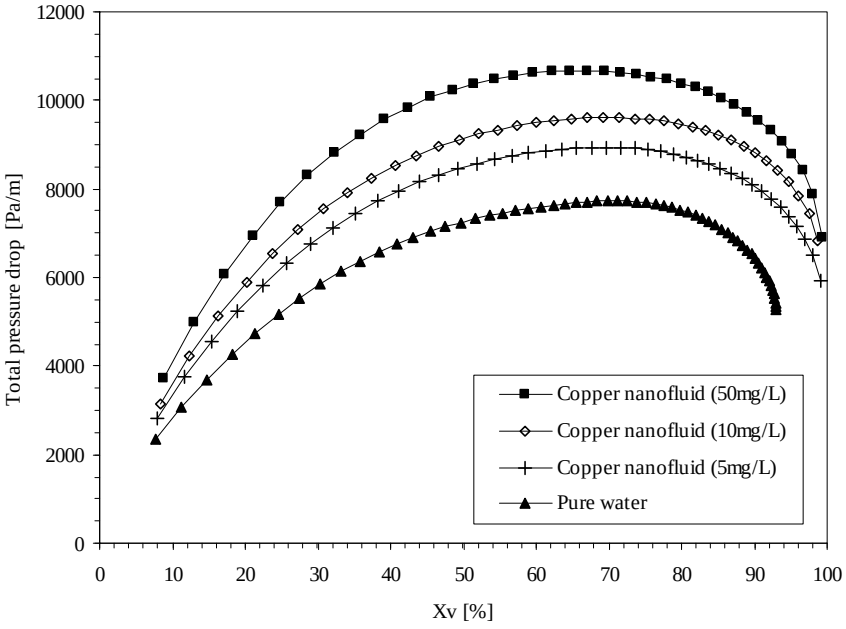

Figure 17. Effect of Cu nanoparticles concentration on total pressure drop.

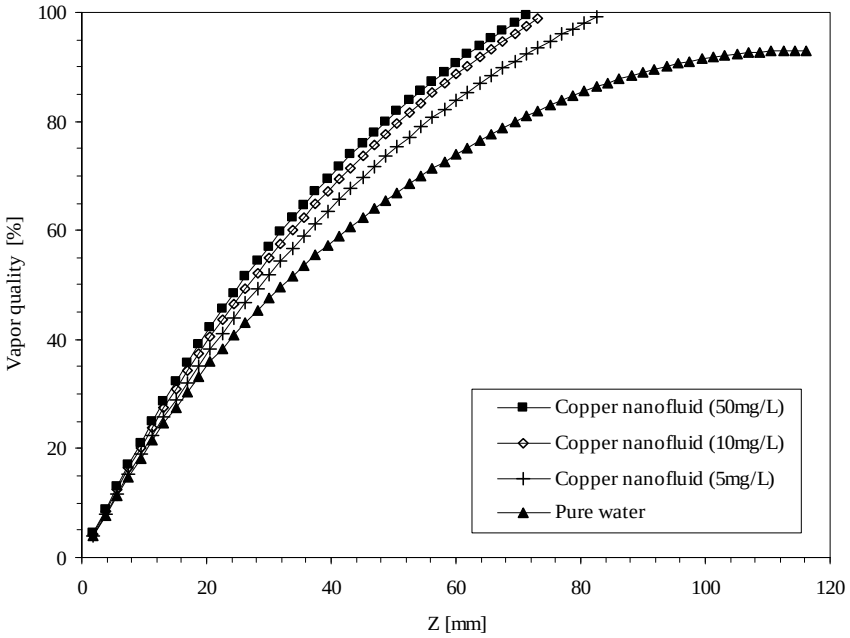

Figure 18. Effect of Cu nanoparticles concentration on local vapor quality